Fujii et al. Radiation Oncology 2011, 6:8
http://www.ro-journal.com/content/6/1/8

RADIATION ONCOLOGY

RESEARCH Open Access

Cationized gelatin-HVJ envelope with sodium borocaptate improved the BNCT efficacy for liver tumors *in vivo*

Hitoshi Fujii[1], Akifumi Matsuyama[2], Hiroshi Komoda[1], Masao Sasai[2], Minoru Suzuki[3], Tomoyuki Asano[4], Yuichiro Doki[1], Mitsunori Kirihata[4], Koji Ono[3], Yasuhiko Tabata[5], Yasufumi Kaneda[6], Yoshiki Sawa[1], Chun Man Lee[1,2,7*]

Abstract

Background: Boron neutron capture therapy (BNCT) is a cell-selective radiation therapy that uses the alpha particles and lithium nuclei produced by the boron neutron capture reaction. BNCT is a relatively safe tool for treating multiple or diffuse malignant tumors with little injury to normal tissue. The success or failure of BNCT depends upon the ^{10}B compound accumulation within tumor cells and the proximity of the tumor cells to the body surface. To extend the therapeutic use of BNCT from surface tumors to visceral tumors will require ^{10}B compounds that accumulate strongly in tumor cells without significant accumulation in normal cells, and an appropriate delivery method for deeper tissues.

Hemagglutinating Virus of Japan Envelope (HVJ-E) is used as a vehicle for gene delivery because of its high ability to fuse with cells. However, its strong hemagglutination activity makes HVJ-E unsuitable for systemic administration. In this study, we developed a novel vector for ^{10}B (sodium borocaptate: BSH) delivery using HVJ-E and cationized gelatin for treating multiple liver tumors with BNCT without severe adverse events.

Methods: We developed cationized gelatin conjugate HVJ-E combined with BSH (CG-HVJ-E-BSH), and evaluated its characteristics (toxicity, affinity for tumor cells, accumulation and retention in tumor cells, boron-carrying capacity to multiple liver tumors *in vivo*, and bio-distribution) and effectiveness in BNCT therapy in a murine model of multiple liver tumors.

Results: CG-HVJ-E reduced hemagglutination activity by half and was significantly less toxic in mice than HVJ-E. Higher ^{10}B concentrations in murine osteosarcoma cells (LM8G5) were achieved with CG-HVJ-E-BSH than with BSH. When administered into mice bearing multiple LM8G5 liver tumors, the tumor/normal liver ratios of CG-HVJ-E-BSH were significantly higher than those of BSH for the first 48 hours ($p < 0.05$). In suppressing the spread of tumor cells in mice, BNCT treatment was as effective with CG-HVJ-E-BSH as with BSH containing a 35-fold higher ^{10}B dose. Furthermore, CG-HVJ-E-BSH significantly increased the survival time of tumor-bearing mice compared to BSH at a comparable dosage of ^{10}B.

Conclusion: CG-HVJ-E-BSH is a promising strategy for the BNCT treatment of visceral tumors without severe adverse events to surrounding normal tissues.

* Correspondence: tg4c_1211@hetp.med.osaka-u.ac.jp
[1]Department of Surgery, Osaka University Graduate School of Medicine, Osaka, Japan
Full list of author information is available at the end of the article

Background

Boron neutron capture therapy (BNCT) is a cell-selective radiation therapy that uses alpha particles and lithium nuclei produced by the boron neutron capture reaction. These particles cause cell destruction, bouncing out to a maximum distance of 10 μm from the target, a distance that corresponds to the size of a cell. These particles only destroy the cells that take up ^{10}Boron (^{10}B) [1]. This therapy is clinically indicated for multiple and diffuse tumors, such as glioblastoma and head and neck tumors [2]. BNCT was recently evaluated for treating liver tumors [3-8], although the prognosis of patients treated by BNCT with conventional ^{10}B compounds, particularly sodium borocaptate (BSH), is not good because of its low accumulation in liver tumors and the attenuation of the epithermal neutron beams directed toward deep lesions [9-11]. Therefore, treating liver tumors effectively with BNCT will require novel ways of delivering BSH, with the characteristics of high accumulation in the tumor, low toxicity for normal tissue, and rapid withdrawal from normal tissue and the bloodstream [12]. Various carriers such as liposomes have been investigated [13-16], but until now a vector for BSH that adequately satisfies the above requirements has not been developed.

Liver tumors, including primary and secondary tumors, are the fifth most common solid tumor worldwide. The incidence is increasing rapidly in most countries, at a pace that will make liver tumors the third most common tumor by 2030 [17,18]. The mortality rate of liver tumors, especially multiple metastatic liver tumors, is high. Multimodal therapies for multiple liver tumors have advanced considerably, and include radiofrequency ablation, radiation, surgical extirpation and transplantation [19]. However, therapy for multiple and diffuse liver tumors is still difficult, because reducing the liver volume reduces its organ function. Therefore, a therapy selective for tumors with minimal damage to normal liver tissue is of great interest.

Hemagglutinating Virus of Japan Envelope (HVJ-E) is a simple vector that is converted into an inactivated virus containing lipid envelope for gene transfer vector originally [20]. HVJ-E has been used to carry anticancer drugs with some success [21,22]. HVJ-E is reported both to possess high fusion ability and to elicit anti-tumor immune responses [23,24], making it an attractive candidate for widespread use in cancer therapy. On the other hand, HVJ-E has strong hemagglutination activity, making it unsuitable to administer systemically. There are no reports describing the systemic administration of HVJ-E in cancer therapy, although one study reports improved HVJ-E stability in the bloodstream when it is administered with a cationized gelatin [25]. The development of a novel HVJ-E-based vector that can be administered into the general circulation is highly desirable for cancer treatment.

We therefore focused on HVJ-E because of its versatility, its high fusion ability, and its ability to stimulate an immune response. We developed a cationized gelatin conjugate of HVJ-E with BSH that can be administered into the general circulation, and we evaluated its safety, bio-distribution, and effectiveness in BNCT treatment using a murine model of multiple liver tumors.

Materials and methods

Mice

Female C3H/HeN Jcl mice at 8-12 weeks of age were obtained from CLEA Japan (Tokyo, Japan) and kept in standard housing. Body weight of mice was 19.6 ± 1.6 (17-23) g at each experiment. All animal experiments were performed under a protocol approved by the Ethics Review Committee for Animal Experimentation of Osaka University Graduate School of Medicine.

Cell line

The cell line of murine osteosarcoma (LM8G5), which was isolated from LM8 cells after five successive cycles of *in vivo* selection procedures, were used because of their high potential for metastasizing to the liver [26,27]. The cells were maintained in D-MEM (Sigma Aldrich Japan, Tokyo, Japan) containing 10% fetal bovine serum, 1% (v/v) 100 × non-essential amino acids, 1 mM sodium pyruvate, 2 mM L-glutamine, 50 μM 2-mercaptoethanol, 100 units/ml penicillin, and 100 μg/ml streptomycin.

Animal Model

LM8G5 cells (1×10^6 cells in 200 μl, with serum-free medium) were injected into the surgically exposed ileocolic vein of mice under general anesthesia with Avertin (2.5% tribromoethanol at a concentration of 1 ml/100 g live weight). Multiple small liver tumors were observed seven days after the injection by exploratory laparotomy, and these tumors led to the death of the mice within 20 days after tumor inoculation.

HVJ-E

HVJ was purified from chicken egg chorioallantoic fluid by centrifugation, and the titer calculated as previously described [20]. The virus was inactivated by UV irradiation exposure (99 mJ/cm^2) just before use, eliminating the ability of the virus to replicate while leaving its fusion capacity intact, as previously described [20].

Cationized Gelatin (CG) and BSH

Gelatin was prepared from pig skin type I collagen through an acid process, and was kindly supplied by Nitta Gelatin (Osaka, Japan). Ethylenediamine (ED),

glutaraldehyde, 2,4,6-trinitrobenzenesulfonic acid, β-alanine, and a protein assay kit (# L8900) were purchased from Nacalai Tesque (Kyoto, Japan). The coupling agent, 1-ethyl-3-(3-dimethylaminopropyl) carbodiimide hydrochloride salt (EDC), was obtained from Dojindo Laboratories (Kumamoto, Japan). The CG was prepared by introducing ED to the carboxyl groups of low-molecular-weight gelatin (M.W. 3,100), as previously described [28]. Sodium borocaptate (Na_2 $^{10}B_{12}H_{11}SH$: BSH), was obtained from Stella Chemifa (Osaka, Japan).

Incorporation into HVJ-E

To incorporate plasmid DNA or BSH into HVJ-E, 10 μl of HVJ-E suspension (1.0×10^{10} particles) was added to 15 μl of 1% protamine sulfate, and this was mixed with plasmid DNA (200 μg) or BSH (6,667 μg boron) and 40 μl of 3% Tween-80 diluted with TE solution (10 mM Tris-HCl, pH 8.0, 1 mM EDTA). Qdot 655 ITK Carboxyl Quantum Dots (Qdot; Invitrogen, Carlsbad, CA, USA) were introduced into HVJ-E by electroporation (250 V, 750 μF). The mixture was centrifuged at 15,000 rpm for 15 min at 4°C. To remove the detergent and unincorporated plasmid DNA, BSH, or Qdot, the pellet was washed with 1 ml of balanced salt solution (10 mM Tris-HCl, pH 7.5, 137 mM NaCl, and 5.4 mM KCl), and the envelope vector was suspended in 1,000 μl of phosphate-buffered saline (PBS). To determine the ^{10}B concentration in the HVJ-E combined with BSH, the complex was digested with nitric acid solution at Bio Research (Hyogo, Japan) and assayed with inductively coupled plasma-atomic emission spectrometry (ICP-AES, ULTIMA2, Horiba Jobin Yvon, Kyoto, Japan).

Cationized Gelatin conjugate HVJ-E (CG-HVJ-E)

The CG-HVJ-E complex was formed by mixing the two materials in an aqueous solution. Briefly, 750 μg of CG was added to 150 μl of 0.1 M PBS (pH 7.4) containing 4.5×10^9 particles of HVJ-E. The solution was mixed by tapping several times. The solution was then incubated on ice for 15 min to form CG-HVJ-E. The CG-HVJ-E vector was purified by centrifugation as described above.

Zeta potential and particle size of HVJ-E compounds

The zeta potential of each HVJ-E complex (HVJ-E, CG-HVJ-E, HVJ-E-BSH, and CG-HVJ-E-BSH) was measured by an electrophoretic light scattering (ELS) assay (ELS-7000AS, Otsuka Electric Co. Ltd., Osaka, Japan) at 37°C with an electric field strength of 100 V/cm [29]. The particle size of each compound was measured by a dynamic light scattering (DLS) assay (Submicron Particle Analyzer N5, Beckman Coulter, Fullerton, CA, USA).

Transmission microscopy

Ultra-thin layers of HVJ-E, CG-HVJ-E, and CG-HVJ-E-BSH stained with 3% uranylacetate were examined with an electron microscope (H-7650 and S-800, Hitachi, Tokyo, Japan) to determine the particle size.

Hemagglutination assay

The hemagglutination assay was done in a 96-well round-bottom plate using 50 μl/well of a 0.5% suspension of chicken red blood cells (Nippon Bio-Test Laboratories, Tokyo, Japan) and 50 μl/well of an HVJ-E solution serially diluted with PBS [30].

Acute toxicity in normal mice

Each HVJ-E complex was administered by intra-cardiac injection (200 μl) into 8-12-week-old female C3H/HeN mice, which were monitored for 7 days for survival.

Blood chemistry monitoring after systemic administration of HVJ-E complexes

Indications of systemic injury were recorded, including serum levels of total bilirubin (T. Bil), aspartate aminotransferase (AST), and alanine aminotransferase (ALT) as markers of liver function, lactate dehydrogenase (LDH) and blood urea nitrogen (BUN) as markers of hemagglutination, and creatinine (Cr) as a marker of renal function. All marker levels were measured using an automated analyzing system (BML, Tokyo, Japan) at 24 and 48 hours and at 7 days after systemic administration of 4.5×10^9 HVJ-E particles.

Affinity of HVJ-E complexes to tumor cells and localization of Qdot carried in HVJ-E complexes

HVJ-E (1.5×10^9 particles) and CG (250 μg) were combined to produce CG-HVJ-E. LM8G5 cells (2×10^4) were seeded into each well of an 8-well Lab-tek chamber (Nalge Nunc International, Rochester, NY, USA) and cultured overnight. The cells were incubated with Qdot alone or Qdot with HVJ-E or CG-HVJ-E, at a concentration of 2.5×10^8 Qdot particles per well for 1 hour. The cells were washed twice with PBS and fixed with 4% paraformaldehyde. Hoechst 33342 (10 μM, Invitrogen) was used to stain the nuclei, and the cells were viewed with fluorescence microscopy (BX61, Olympus, Tokyo, Japan). To visualize the intracellular localization of the Qdot carried in the HVJ-E or CG-HVJ-E, the cells were stained with Hoechst 33342 for the nucleus and Alexa Fluor 488 phalloidin (Invitrogen) for the cytoplasm, and were viewed by confocal microscopy (Fluoview FV1000, Olympus).

Transfection efficiency of HVJ-E complexes into tumor cells

The various HVJ-E complexes were incubated with tumor cells to evaluate their transfection efficiency. LM8G5 cells (2×10^4) were seeded into each well of a 96-well plate, cultured overnight with 200 μl of culture medium, and washed with PBS. Each HVJ-E complex

with or without luciferase-expressing plasmids (50 μl; 1.5×10^9 particles) was incubated with tumor cells for 30 min, and then incubated for 30 min at 37°C. After washing twice with PBS, the cells were incubated with fresh medium for 24 hours and then lysed with Lysis Buffer (Promega, Madison, WI, USA). Luciferase activity in the cells was then measured with a Luciferase Assay kit (Promega) using a fluorescence plate reader (Mithras LB 940, Berthold Technologies, Bad Wildbad, Germany). The protein content of the samples was assayed by the Bradford method [31].

Accumulation and retention of BSH or CG-HVJ-E-BSH in tumor cells *in vitro*

Tumor cells of the LM8G5 cell line (1×10^6) were seeded in 75 cm^2 tissue culture flasks and were cultured overnight. The cells were then washed with PBS, 1 ml of BSH (20 μg boron/ml) or CG-HVJ-E-BSH (20 μg boron/ml) was added to each flask, and the mixture was incubated for 30 min at 37°C. The cells were then washed twice with PBS, and the ^{10}B concentration in the cells was immediately measured by ICP-AES (Horiba Jobin Yvon) as the initial ^{10}B value bound to the cells. Other flasks were incubated an additional 24-48 hours at 37°C and the cells were double-washed again before being tested for ^{10}B concentration, which was measured as the ^{10}B value.

Bio-distribution of BSH or CG-HVJ-E-BSH in normal or liver tumor-bearing mice

Mice were injected with 200 μl of BSH (35 μg boron/g) or 200 μl of CG-HVJ-E-BSH (1.2 μg boron/g), administered into the general circulation. At 1, 24, or 48 hours after the injection, mice were sacrificed and peripheral blood samples collected. The lung, liver, kidney and spleen were removed after whole-body perfusion with heparinized saline, and weighted. The extracted tissues were digested with the M-Per mammalian protein extraction reagent (Pierce Chemical Co., Rockford, IL, USA) and ultrasonic homogenizer (H3-350, Kawajiri Machinery, Hyogo, Japan), and the ^{10}B concentration in each sample was measured by ICP-AES (Horiba Jobin Yvon). The ^{10}B accumulation into each organ was calculated as the percentage of ^{10}B per weight of each organ.

Neutron capture autoradiography imaging of murine liver sections after BSH or CG-HVJ-E-BSH administration

Mice bearing liver tumors were given either 35 μg boron/g of BSH or 1.2 μg boron/g of CG-HVJ-E-BSH, administered into the general circulation. The mice were sacrificed 1 hour after BSH administration or 24 hours after CG-HVJ-E-BSH administration. The liver was removed after whole-body perfusion with heparinized saline. Frozen 16-μm-thick liver sections were mounted on Baryotrak-P detector plates (Nagase-Landauer, Tokyo, Japan) and air-dried for 60 min. The samples were exposed to thermal neutrons at a rate of 2.1×10^{13} neutrons/$m^2 \cdot s^1$ for 1 hour at the Japan Research Reactor 4 (JRR-4). For α-auto-radiographic imaging, the detector plates were etched in 7 N NaOH at 70°C for 2 hours to reveal the proton tracks produced by the boron neutron capture reaction [32]. The number of α particles per 10,000 μm^2 in each section was counted using VH Analyzer software (Biozero, Keyence, Osaka, Japan).

Antitumor efficacy of BNCT for murine liver tumors with BSH or CG-HVJ-E-BSH

Mice bearing liver tumors were irradiated with a thermal neutron beam at the JRR-4 8 days after tumor cell inoculation. The mice were given 1.2 μg boron/g of CG-HVJ-E-BSH 24 hours before irradiation treatment, or 35 μg boron/g of BSH 1 hour before irradiation treatment, administered into the general circulation. The mice were then set the acrylic stand, and irradiated for 17 min at the Japan Research Reactor 4 (JRR-4). Neutron irradiation was performed in a single fraction using an thermal beam mode I of JRR-4. In the in-air beam characteristics, thermal neutron flux and the γ-ray absorbed dose were 2.1×10^{13} neutrons/$m^2 \cdot s^1$ and 3.6 Sv/h at a reactor power of 3.5 MW, respectively. To evaluate the effect of BNCT treatment on the liver tumors, the mice were sacrificed 6 days after irradiation, and the livers removed, weighed, and evaluated for pathologic changes. In a separate experiment, 1.2 μg boron/g of BSH or 1.3 μg boron/g of CG-HVJ-E-BSH was administered, the mice were either irradiated or not, and their survival time after irradiation was recorded.

Statistical analyses

Student's *t*-test was used to determine whether the differences between the various groups were significant. Differences between groups in the survival experiment were determined using the Kaplan-Meier log-rank test. A *p*-value of less than 0.05 was considered statistically significant.

Results

CG-HVJ-E characteristics

SDS-PAGE results confirmed that when mixed and centrifuged with HVJ-E, the CG bound to HVJ-E in a dose-dependent manner within a certain range (data not shown). The optimal ratio of CG to HVJ-E, in which the CG-HVJ-E containing luciferase plasmid was transferred most efficiently into LM8G5 cells (data not shown), was identified as 1 μg to 6.0×10^6 particles, and the zeta potential and particle size of the resulting CG-HVJ-E conjugate was measured (Table 1). CG- HVJ-E was

Table 1 Zeta potential and particle sizes of each HVJ-E complex

Complex	Apparent molecular size (nm)	Zeta potential (mV)
HVJ-E	293 ± 32	-25 ± 1
CG-HVJ-E	297 ± 21	-15 ± 3
HVJ-E-BSH	448 ± 144	-28 ± 1
CG-HVJ-E-BSH	494 ± 196	-19 ± 2

more positive (-14.7 mV) than HVJ-E (-25.1 mV). The form and size of these particles were estimated by using Transmission Electron Microscopy (TEM) and Scanning Electron Microscopy (SEM). HVJ-E, CG-HVJ-E, and CG-HVJ-E-BSH were approximately 300, 300, and 500 nm in diameter, respectively, as measured by TEM (Additional file 1, Figure S1). The DLS assay results were similar (data not shown). Therefore, these data are able to give an estimate that incorporating BSH into the HVJ-E complexes made them larger and slightly more positive than either HVJ-E or CG-HVJ-E.

CG-HVJ-E had less hemagglutination activity in vitro and was less toxic than HVJ-E in mice

Hemagglutination is caused by hemagglutinin-neuramidase (HN) protein on the HVJ-E membrane [33]. The hemagglutination of chicken blood cells by CG-HVJ-E was approximately half that of HVJ-E (data not shown). The acute toxicity was determined by administering various concentrations of HVJ-E or CG-HVJ-E to normal mice and monitoring their survival over 7 days; the 100% survival dosage of CG-HVJ-E (6.0×10^9 particles) was higher than that of HVJ-E (4.5×10^9 particles). Blood tests done 24 hours after the administration of 4.5×10^9 particles of HVJ-E or 4.5×10^9 particles of CG-HVJ-E showed that blood chemistry markers in the CG-HVJ-E-treated mice were almost within the normal range, while those in the HVJ-E-treated mice were significantly higher (Figure 1). These levels peaked 24 hours after administration in mice treated with HVJ-E, and became normal at 7 days (data not shown).

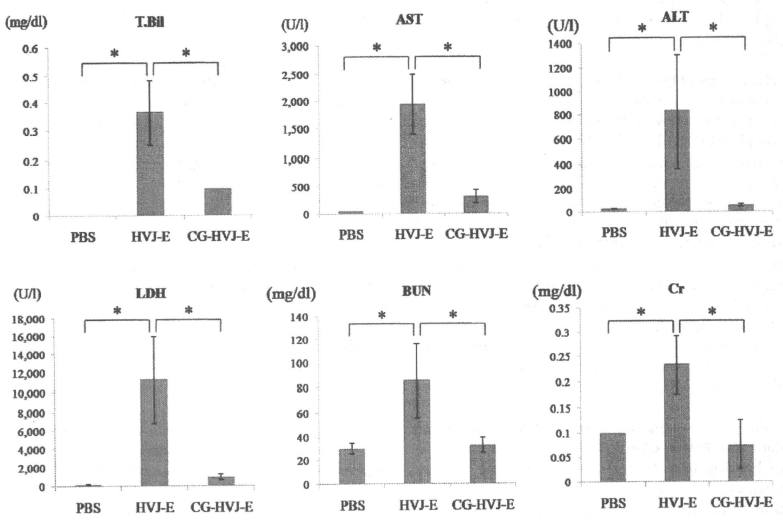

Figure 1 Blood chemistry tests 24 hours after HVJ-E and CG-HVJ-E administration into normal mice. Blood markers (T.Bil, AST, ALT, LDH, BUN, and Cr) in normal mice tested 24 hours after intra-cardiac injection of PBS, HVJ-E or CG-HVJ-E. * $p < 0.05$. Results shown are the means ± SD (n = 4).

High affinity and infusion ability of CG-HVJ-E in tumor cells

CG-HVJ-E containing Qdot had a higher affinity for tumor cells than Qdot alone or HVJ-E containing Qdot (Figure 2A). CG-HVJ-E containing Qdot was taken into the cytoplasm, and some Qdots were localized to the nuclei, as seen by confocal microscopy (Figure 2B).

CG-HVJ-E transfection into tumor cells *in vitro* was highly efficient

CG-HVJ-E's *in vitro* transfection efficiency into tumor cells was 4 times greater than that of HVJ-E, as assessed by a luciferase assay, and it was not cytotoxic (Figure 2C). The enhanced transfection efficiency of CG-HVJ-E was also observed in another tumor cell line (CT26: murine colon cancer, data not shown).

CG-HVJ-E-BSH increased ^{10}B accumulation and retention in tumor cells *in vitro* compared to BSH

The concentration of ^{10}B was significantly higher in cells incubated with CG-HVJ-E-BSH than in those incubated with BSH ($p < 0.05$). The ^{10}B levels gradually decreased in both cell groups, but the levels were significantly higher in the cells incubated with CG-HVJ-E-BSH than

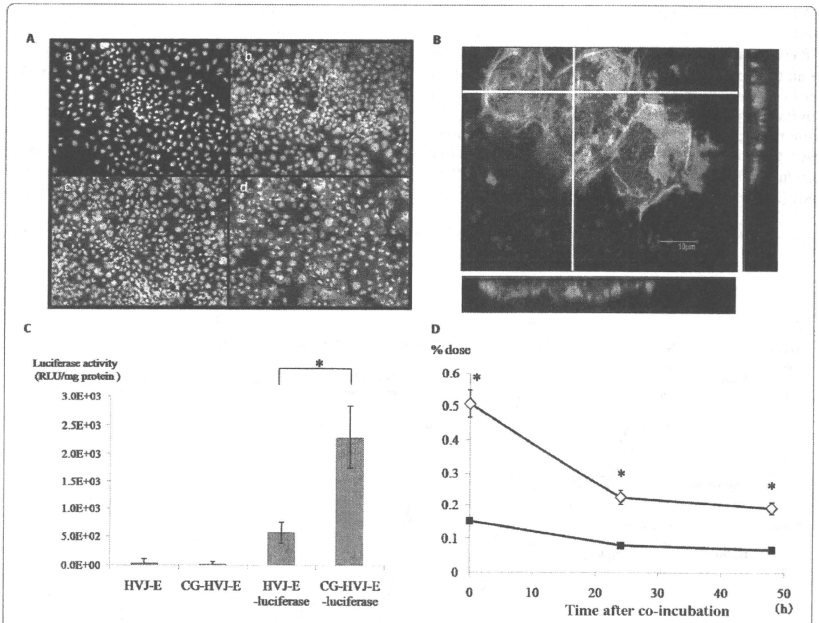

Figure 2 Affinity of CG-HVJ-E for tumor cells and the intracellular uptake of molecules incorporated into HVJ-E. A) Affinity of HVJ-E and CG-HVJ-E for tumor cells. LM8G5 cells were incubated alone (a), or with Qdot (b), HVJ-E-Qdot (c), or CG-HVJ-E-Qdot (d) for 60 min in a Lab-tek chamber slide and examined for Qdot (red) and Hoechst 33342 (blue) by fluorescence microscopy. Representative views are shown. B) Intracellular localization of Qdot transported by CG-HVJ-E. Tumor cells were incubated with CG-HVJ-E-Qdot (orange) and stained with Hoechst 33342 (blue) and Alexa Fluor 488 phalloidin (green). Image shows 3-dimensional analysis with confocal microscopy. C) Luciferase activity in tumor cells transfected with HVJ-E or CG-HVJ-E. Cells were cultured for 30 min with HVJ-E or CG-HVJ-E containing a luciferase-expressing plasmid. Luciferase activity was measured 24 hours later to evaluate the transfection efficiency. Results are shown as means ± SD (n = 4). Similar results were obtained in three experiments. * $p < 0.05$. D) ^{10}B accumulation and retention in tumor cells *in vitro*. Cells were incubated with 20 μg boron/ml of BSH or CG-HVJ-E-BSH for 30 min, then washed twice with PBS, and the ^{10}B concentration was measured by ICP-AES. Separately, cells were incubated in the same manner, but after washing, were incubated in medium without BSH for 24 or 48 hours before testing for ^{10}B concentration as described above. The horizontal axis shows time after co-incubation. The vertical axis shows the percent of the administered dose (% dose) of CG-HVJ-E-BSH (open diamond) or BSH (solid square). Results shown are the means ± S.D. (n = 3). * $p < 0.05$.

in those with BSH for at least 48 hours after incubation (Figure 2D). These results indicate that CG-HVJ-E-BSH binds rapidly to tumor cells and that the ^{10}B contained in CG-HVJ-E-BSH is internalized into the cytoplasm or the nucleus. Adding CG-HVJ-E-BSH to tumor cells *in vitro* resulted in sufficient ^{10}B accumulation and retention in the cells to be useful for BNCT.

BSH incorporated into CG-HVJ-E accumulated in liver tumors and rapidly disappeared from normal tissues in tumor-bearing mice

In normal mice, the ^{10}B concentration in the liver 1 hour after administration was higher with BSH than with CG-HVJ-E-BSH. The concentration of both compounds started to decrease by 48 hours after administration. The ^{10}B concentration in the lung, kidney, and spleen was low at all time points with both compounds (Figure 3A). In the liver tumor model, BSH and CG-HVJ-E-BSH behaved similarly in the normal liver tissue surrounding the tumors (Figure 3B, middle panel). In the tumors, however, the concentration of ^{10}B at 1 and 24 hours after administration was significantly higher with CG-HVJ-E-BSH (34.76 and 10.71% dose/g) than with BSH (2.21 and 2.29% dose/g) (Figure 3B, left panel). In the bloodstream, the ^{10}B concentration at 1 hour after administration tended to be higher with CG-HVJ-E-BSH (20.9% dose/ml) than with BSH (7.96% dose/ml), despite the lower quantity of ^{10}B administered with both boron compounds (1.2 μg boron/g). From 24 hours after administration and onward, the concentration of ^{10}B from both compounds was the same (Figure 3B, right panel).

Tumor/Normal liver ^{10}B ratio in murine liver tumors was greater with CG-HVJ-E-BSH

The Tumor/Normal (T/N) liver ^{10}B ratio with CG-HVJ-E-BSH was significantly higher than with BSH from 1 to 48 hours after administration ($p < 0.05$), with a peak difference at 24 hours ($p < 0.05$; Figure 3C). The Tumor/Blood ^{10}B ratio of CG-HVJ-E-BSH also remained higher than that of BSH from 1 to 48 hours after administration (data not shown).

CG-HVJ-E-BSH improved the T/N ^{10}B ratio in neutron capture autoradiography images of murine liver tumors

Neutron capture autoradiography (NCAR) was performed after BSH (35 μg boron/g) or CG-HVJ-E-BSH

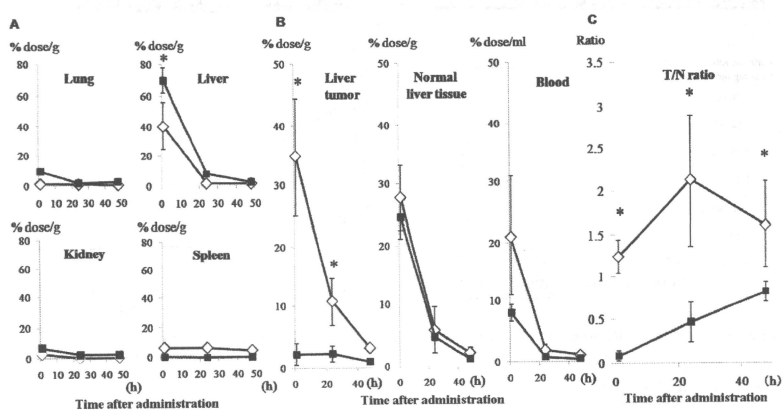

Figure 3 Bio-distribution of ^{10}B in mice with normal liver or with liver tumors. A) Time course of organ (lung, liver, kidney, and spleen) uptake of ^{10}B delivered by 1.2 μg boron/g of BSH or CG-HVJ-E-BSH in normal mice. B) Time course of tumor accumulation (left panel), liver uptake (middle panel), and blood residence (right panel) of ^{10}B delivered by 1.2 μg boron/g of BSH or CG-HVJ-E-BSH in tumor-bearing mice. The horizontal axis shows the time after administration. The vertical axis shows the percent of the administered dose per gram of tissue (% dose/g). C) Time course of the Tumor-to-Normal liver tissue (T/N) ^{10}B concentration ratio for CG-HVJ-E-BSH (open diamond) or BSH solution (solid square). Data are expressed as the mean ± S.D. (n = 3). * $p < 0.05$ compared with BSH.

(1.2 μg boron/g) was injected into mice bearing liver tumors. The ^{10}B particle count in the BSH- and CG-HVJ-E-BSH-treated livers are shown in Figure 4B and 4C. The T/N ratio 1 hour after BSH administration was 0.12, and that for CG-HVJ-E-BSH at 24 hours after administration was 2.76 (Figure 4D), which is similar to the values obtained in the bio-distribution study. It is of interest that the T/N ^{10}B ratio was higher with CG-HVJ-E-BSH, even though the actual quantity of ^{10}B was 30 times greater in the BSH dosage. The number of α particles with CG-HVJ-E (415 ± 35) was similar to that of BSH (451 ± 107) in the liver tumor sections (Figure 4A).

BNCT with CG-HVJ-E-BSH inhibited tumor growth, preserved the normal surrounding liver tissue, and prolonged survival time in the murine liver tumor model

To evaluate the use of BNCT with CG-HVJ-E-BSH for murine liver tumors, BNCT was performed on mice bearing LM8G5 liver tumors. To assess the T/N ratio of CG-HVJ-E-BSH, BNCT was performed 24 hours after CG-HVJ-E-BSH administration or 1 hour after BSH administration [2,4]. We first evaluated the anti-tumor efficacy at 14 days after tumor cell inoculation, because up to that time, the tumor-bearing mice were severely damaged by the radical spread of tumors (about 50% of the untreated mice were dead). Therefore, we sacrificed the tumor-bearing mice that were alive until that time to evaluate the efficacy of BNCT.

BNCT with CG-HVJ-E-BSH (1.2 μg boron/g) inhibited the local growth of liver metastases as much as BNCT with BSH (35 μg boron/g). This dosage of BSH was determined from the clinical dose for BNCT for various malignant tumors, and effectively contained 35 times the ^{10}B that was present in the CG-HVJ-E-BSH dosage (Figure 5A, B). Some histological damage, which appeared, for example as fractionated or vacuolated

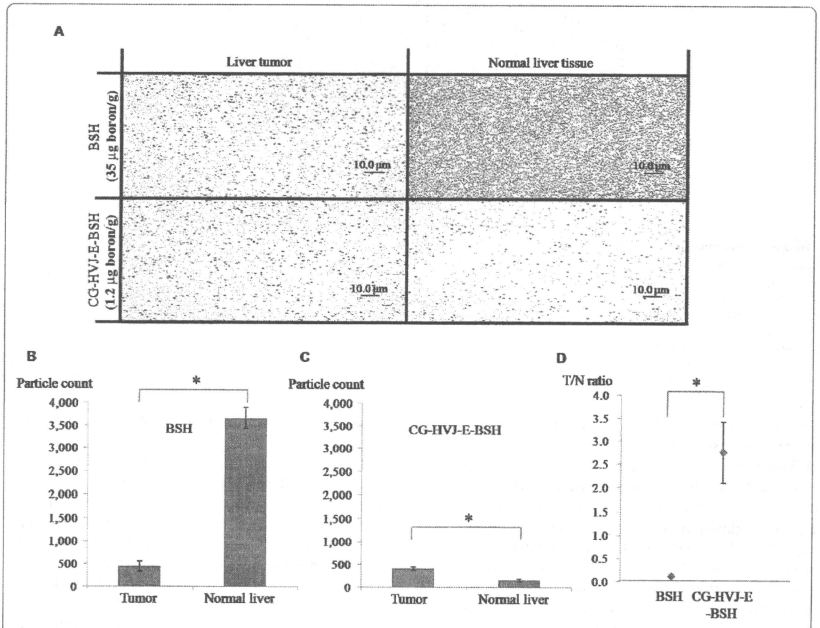

Figure 4 Neutron capture radiographic image in murine liver sections after administration of BSH or CG-HVJ-E-BSH. Liver sections from tumor-bearing mice were prepared and frozen 1 hour after BSH (35 μg boron/g) injection or 24 hours after CG-HVJ-E-BSH (1.2 μg boron/g) injection. The sections were placed on CR-39 detector plates and exposed to thermal neutrons (2.1×10^{13} neutrons/$m^2 s^1$) for 1 hour. A) The number of α particles per 10,000 μm^2 section was counted by VH Analyzer software after NaOH etching. B) The number of α particles per 10,000 μm^2 section of BSH or C) of CG-HVJ-E-BSH (n = 3). D) Tumor-to-normal liver tissue (T/N) ratio for the number of α particles.

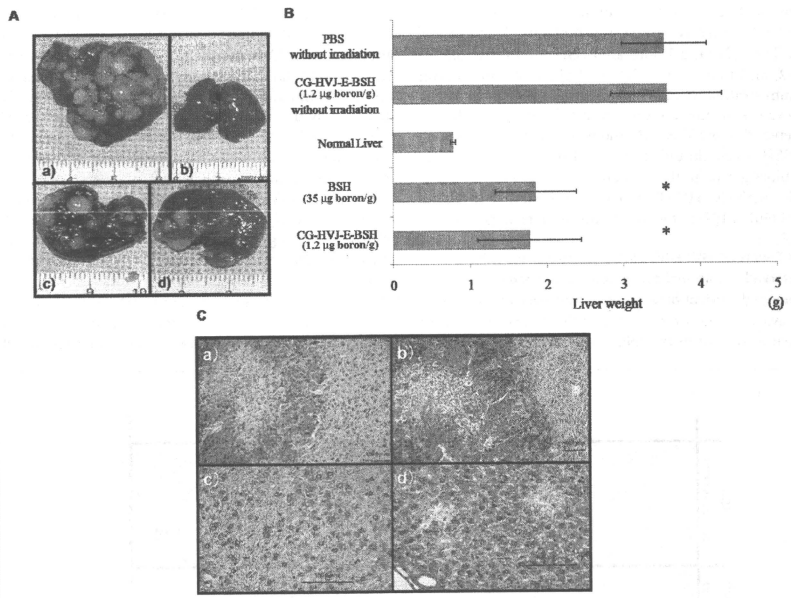

Figure 5 Anti-tumor efficacy of BNCT in mice with liver tumors. C3H/HeN mice were given an intra-portal injection of LM8G5 cells (1×10^6 cells) on day 0. Mice were given a single intra-cardiac injection of CG-HVJ-E-BSH (1.2 μg boron/g) 24 hours before irradiation, or BSH (35 μg boron/g) 1 hour before irradiation. PBS and CG-HVJ-E-BSH solution were administered without neutron irradiation as a control. After irradiation on day 8, mice were sacrificed on day 14 to determine the BNCT efficacy on tumor metastasis. A) Macroscopic views (a) of the liver with tumors after administration of PBS; (b) normal liver; (c) liver with tumors after BNCT with BSH, and (d) liver with tumors after BNCT with CG-HVJ-E. B) Liver weight after BNCT. * $p < 0.05$ compared with PBS or CG-HVJ-E without irradiation. (each group n = 4). C) Representative light microscopic views of liver tumor tissue (upper panels, low magnification) or normal liver tissue (lower panels, high magnification) 6 days after BNCT with CG-HVJ-E-BSH (1.2 μg boron/g) (a, c) or BSH (35 μg boron/g) (b, d). Sections are stained with hematoxylin-eosin. Bar: 100 μm.

cells, was observed in both the tumor mass and in the normal liver tissue after BNCT with BSH (35 μg boron/g) (Figure 5C-b, d). In contrast, little histological damage was detected in the normal liver tissue surrounding the tumors after BNCT with CG-HVJ-E-BSH (Figure 5C-a, d). We originally thought that the damage to the liver might have been influenced by the longer survival time of mice treated with BSH and BNCT; however, the survival rate of these mice at 14 days after tumor cell inoculation was 37.5% (Additional file 2, Figure S2). This survival time was shorter than that of the untreated tumor-bearing mice. As we were not able to be certain if this dosage of BSH was a clinical equivalent, we used a dose of 1.3 μg boron/g of BSH to evaluate the survival time after BNCT, compared to a dose of 1.2 μg boron/g of CG-HVJ-E-BSH.

Finally, we compared the effectiveness of BNCT against tumors when used with BSH or CG-HVJ-E-BSH, in terms of survival after BNCT. With the assumption that the survival time of tumor-bearing mice after BNCT with a high dose of BSH (35 μg boron/g) was affected by normal liver damage as well as anti-tumor efficacy, both compounds were administered at dosages with similar ^{10}B concentrations (CG-HVJ-E-BSH, 1.2 μg boron/g or BSH,1.3 μg boron/g) into mice bearing liver tumors at 24 hours or 1 hour before irradiation, respectively. Irradiation was performed 8 days after the tumor cell inoculation, and the survival of the mice assessed.

CG-HVJ-E-BSH was most effective in increasing the mean survival time of mice bearing liver tumors compared with the other groups ($p < 0.005$; Additional file 2, Figure S2). We observed little histological damage in the normal liver tissues 6 days after BNCT with the lower dose of BSH (1.3 μg boron/g) besides the damage that was already present in the tumor mass (Additional file 3, Figure S3).

Discussion

With the goal of creating a novel BSH vector for effective BNCT, we chose HVJ-E because of its strong fusion ability, its effectiveness as a vehicle for delivering various drugs and genes, and its ability to stimulate an immune response against tumors in local cancer therapy [23]. Clinical trials of locally administered HVJ-E for patients with advanced malignant melanoma are underway in Japan. Although HVJ-E is not suitable for systemic administration because of its strong hemagglutinating activity, it has been reported that combining HVJ-E with 5,000-kDa cationized gelatin greatly improves its stability in the bloodstream [25]. In this study, we developed CG-HVJ-E combined with BSH, which can be administered into the general circulation, unlike HVJ-E, and confirmed its bio-distribution.

We compared the safety and efficacy of CG-HVJ-E-BSH in BNCT with that of BSH, using a murine model for liver tumors. For systemic administration, we developed a smaller CG-HVJ-E with a lower molecular weight (3,300 kDa) CG compared with the previously used CG-HVJ-E, which had a particle diameter of 777 nm [25]. We found that this CG-HVJ-E could be safely administered systemically in mice, with reduced toxicity and hemagglutination compared to HVJ-E (Figure 1). In the bio-distribution test using normal mice, both BSH and CG-HVJ-E-BSH accumulated in the liver immediately, but almost all of the ^{10}B had disappeared from the normal liver 48 hours later (Figure 3A). In liver tumors, however, CG-HVJ-E-BSH accumulation was greater than that of BSH although the boron proceeding from CG-HVJ-E-BSH was 35 times higher than that of BSH (Figure 3B); accordingly, the CG-HVJ-E-BSH T/N ratio was significantly higher than that of BSH in tumor-bearing mice, particularly at 24 hours after administration (Figure 3C). Neutron capture autoradiography revealed a higher T/N ^{10}B ratio with CG-HVJ-E-BSH than with BSH 1 hour after administration, despite the 35-fold-higher quantity of ^{10}B contained in the BSH dosage (Figure 4).

In our experiments, BNCT was performed 1 hour after BSH administration, because it followed the reported procedure for the clinical use of BNCT for liver tumors [9], and there was little difference between the T/N ratio an hour after administration and the ratio over the next 24 hours (Figure 3C). This was due to the protracted circulating time of CG-HVJ-E-BSH in the bloodstream. Therefore, this complex accumulated in the tumor by the enhanced permeability and retention (EPR) effect [34]. In fact, the particle size of the CG-HVJ-E-BSH was suitable for the EPR effect (Table 1) [35]. Another reason for this finding was that CG-HVJ-E has a high affinity and high fusion ability for tumor cells (Figure 2A, B, C). Although ^{10}B was taken up by the tumor cells over time, a large number of CG-HVJ-E-BSH molecules were incorporated into the tumor cells immediately, and high ^{10}B concentrations were maintained much longer with CG-HVJ-E-BSH than with BSH (Figure 2D). The mechanism for the preferential affinity of CG-HVJ-E to tumor cells as compared with HVJ-E has not been clarified, but it has been reported that when HVJ-E is conjugated with cationized gelatin, the transfection efficiency improves without a loss of cell fusion ability [25]. Therefore, the efficacy of CG-HVJ-E-BSH was similar to the 35-fold higher dose of ^{10}B as BSH for suppressing the spread of tumor cells without normal liver injury (Figure 5A, B, C).

When used in BNCT, the CG-HVJ-E-BSH significantly increased the survival time over BSH at an equivalent ^{10}B dosage (Additional file 2, Figure S2). Generally, BSH is rarely transferred into the cytoplasm and, once there, is easily removed [36]. On the other hand, CG-HVJ-E-BSH was highly selective for tumor cells and showed both strong fusion ability and the ability to transfer into the tumor cell nucleus. As a result, CG-HVJ-E-BSH improved the effectiveness of BNCT because the ^{10}B was highly concentrated and retained in the nuclei of the tumor cells (Figure 2B, C), where its cytotoxicity was much higher than that of ^{10}B bound to the tumor cell surface [14,37,38].

Moreover, HVJ-E has the potential to induce a bystander effect, so that CG-HVJ-E-BSH could be incorporated into vicinal cells through gap junctions. It is possible that BNCT with CG-HVJ-E-BSH induces a synergistic effect, resulting in a greater destruction of vicinal tumor cells than is seen with BNCT with BSH, which induces a bystander effect that generates hereditary abnormalities in vicinal cells [39].

We chose multiple liver tumors as a target for evaluating the effectiveness of BNCT with CG-HVJ-E-BSH, because BNCT for multiple liver tumors has not gained popularity and the T/N ratio needs to be improved for deep-site tumors. In the absence of liver function disorders, the response of multiple liver tumors is thought to be a good indication of BNCT effectiveness. In this report, we treated mice bearing liver tumors with BNCT [27] after establishing the presence of tumors of several millimeters in diameter. This murine model appears to reflect the clinical stage that we targeted. BNCT with BSH is not indicated for multiple liver tumors in clinical

settings and is only at the experimental stage [9,10]. BNCT was significantly more effective against liver tumors when used with CG-HVJ-E-BSH than with BSH, and normal liver tissue was not injured. The limited injury to normal liver tissue makes more than one BNCT irradiation possible, which is likely to increase the therapeutic potential. However, in these experiments, only one irradiation was done. With regard to BNCT with BSH for clinical liver tumors at deep sites, the required T/N ^{10}B ratio is over 15 [36,40]. Moreover, the human trunk is much thicker than the murine trunk. Therefore, for BNCT with CG-HVJ-E-BSH to become an established, effective clinical procedure, further improvements are needed not only in the drug-delivery system, but also in the vessel-selective delivery [41] because of the attenuation of neutron beams directed toward deep lesions.

Our trial of BNCT for multiple liver tumors at deep sites should forward its development to treat other deep-site tumors, such as pancreatic cancer and malignant mesothelioma [42-44], and further the investigation into BNCT and HVJ-E. However, some problems need to be resolved in future experiments, particularly with regard to improving the incorporation of ^{10}B into the HVJ-E.

It has been reported that locally administered HVJ-E induces immuno-responses against tumors [23. 24], and effectively transports antitumor drugs [22,45]. Our experiments included a single administration of HVJ-E, which did not appear to have an anti-tumor effect unless accompanied by irradiation (Figure 5B, Additional file 2, Figure S2). However, the fractionated administration of HVJ-E, as is used for other vaccinations, might be possible. To address the limitations of this novel HVJ-E BSH, investigations into concurrent chemo-radiation therapy, fractionated administration with or without ^{10}B, and conjugating with ligands for tumor-specific molecules should be performed.

In summary, we developed a form of CG-HVJ-E that could be administered into the general circulation and had both high tumor selectivity and high retention in tumor cells. This vector, when combined with BSH, improved the efficacy of BNCT for multiple liver tumors *in vivo*. Therefore, CG-HVJ-E holds potential for a drug delivery system with clinical applications for cancer therapy.

Additional material

Additional file 1: Figure S1. Transmission electron microscope photographs of HVJ-E complexes. (A) HVJ-E, (B) CG-HVJ-E, and (C) CG-HVJ-E-BSH. Bar: 200 nm.

Additional file 2: Figure S2. Survival of mice treated with BNCT. Mice were given a single intra-cardiac injection of CG-HVJ-E-BSH (1.2 μg boron/g) 24 hours before irradiation, or BSH (1.3 μg boron/g) 1 hour before irradiation. PBS and CG-HVJ-E-BSH were administered without irradiation as a control. The mean survival time of the mice that received the BNCT treatment with CG-HVJ-E-BSH was significantly longer than that of the other groups (n = 4). * $p < 0.005$ (PBS without neutron irradiation, 1.3 μg boron/g of BSH with neutron irradiation, 1.2 μg boron/g of CG-HVJ-E-BSH without neutron irradiation vs. 1.2 μg boron/g of CG-HVJ-E-BSH with neutron irradiation).

Additional file 3: Figure S3. Representative light microscopy views of the liver tumor (A) and normal liver tissue (B) 6 days after BNCT with a low dose of BSH (1.3 μg boron/g). Tissues were stained with hematoxylin-eosin. Bar: 100 μm.

Abbreviations

BNCT: Boron Neutron Capture Therapy; BSH: sodium borocaptate; HVJ-E: Hemagglutinating Virus of Japan Envelope.

Acknowledgements

This work was supported in part by a grant for research and development of a Fixed Field Alternating Gradient Accelerator and DDS for BNCT from the New Energy and Industrial Technology Development Organization (NEDO), a Health Labour Science Research Grant from the Ministry of Health, Labour and Welfare of Japan, and a grant-in-Aid for Exploratory Research from the Ministry of Education, Culture, Sports, Science and Technology (MEXT).

Author details

[1]Department of Surgery, Osaka University Graduate School of Medicine, Osaka, Japan. [2]Medical Center for Translational Research, Osaka University Hospital, Osaka, Japan. [3]Particle Radiation Oncology Research Center Laboratory, Research Reactor Institute, Kyoto University, Osaka, Japan. [4]Department of Agriculture, Osaka Prefectural University, Osaka, Japan. [5]Department of Biomaterials, Institute for Frontier Medical Sciences, Kyoto University, Kyoto, Japan. [6]Division of Gene Therapy Science, Osaka University Graduate School of Medicine, Osaka, Japan. [7]Health Care Economics and Industrial Policy, Osaka University Graduate School of Medicine, Osaka Japan.

Authors' contributions

HF carried out the study, and contributed to the conception of the manuscript and the interpretations of the data. AM, HK, MS, MS, AT, and YT participated in the design of the study. YD, MK, and KO provided some intellectual recommendation. YK and YS provided some intellectual recommendation and reviewed the manuscript. CML conceived of the study, and participated in its design and coordination. All authors read and approved the final manuscript.

Competing interests

All authors declare there were no actual or potential conflicts of interest in this study.

Received: 17 October 2010 Accepted: 20 January 2011
Published: 20 January 2011

References

1. Barth RF, Coderre JA, Vicente MG, Blue TE: **Boron neutron capture therapy of cancer: current status and future prospects.** *Clin Cancer Res* 2005, 11:3987-4002.
2. Yamamoto T, Nakai K, Matsumura A: **Boron neutron capture therapy for glioblastoma.** *Cancer Lett* 2008, 262:143-52.
3. Pinelli T, Zonta A: **From the first idea to the application to the human liver.** Research and development in Neutron Capture Therapy; 2002.
4. Suzuki M, Sakurai Y, Hagiwara S, Masunaga S, Kinashi Y, Nagata K, Maruhashi A, Kudo M, Ono K: **First attempt of boron neutron capture therapy (BNCT) for hepatocellular carcinoma.** *Jpn J Clin Oncol* 2007, 37:376-81.
5. Wittig A, Malago M, Collette L, Huiskamp R, Buhrmann S, Nievaart V, Kaiser G, Jockel KH, Sauerwein W: **BNCT in liver metastases: results of the EORTC trial 11001.** *Strahlentherapie Und Onkologie* 2007, 183:115-115.
6. Sauerwein W, Malago M, Moss R, Altieri S, Hampel G, Wittig A, Nievaart V, Collette L, Mauri P, Huiskamp R, Michel J, Daquino G, Gerken G, Bornfeld N, Broelsch CE: **Boron Neutron Capture Therapy (BNCT) for the treatment of**

diffuse, non-resectable liver metastases. *Strahlentherapie Und Onkologie* 2006, **182**:109-109.

7. Cardose JE, Trivillin VA, Heber EM, Nigg DW, Calzetta O, Blaumann H, Longhino J, Itoiz ME, Bumaschny E, Pozzi E, Schwint AE: **Effect of Boron Neutron Capture Therapy (BNCT) on normal liver regeneration: Towards a novel therapy for liver metastases.** *International Journal of Radiation Biology* 2007, **83**:699-706.
8. Chou FI, Chung HP, Liu HM, Chi CW, Lui WY: **Suitability of boron carriers for BNCT: Accumulation of boron in malignant and normal liver cells after treatment with BPA, BSH and BA.** *Applied Radiation and Isotopes* 2009, **67**:5105-108.
9. Wittig A, Malago M, Collette L, Huiskamp R, Buhrmann S, Nievaart V, Kaiser GM, Jockel KH, Schmid KW, Ortmann U, Sauerwein WA: **Uptake of two ^{10}B-compounds in liver metastases of colorectal adenocarcinoma for extracorporeal irradiation with boron neutron capture therapy (EORTC Trial 11001).** *Int J Cancer* 2008, **122**:1164-71.
10. Suzuki M, Masunaga SI, Kinashi Y, Takagaki M, Sakurai Y, Kobayashi T, Ono K: **The effects of boron neutron capture therapy on liver tumors and normal hepatocytes in mice.** *Jpn J Cancer Res* 2000, **91**:1058-64.
11. Sakurai Y, Ono K, Miyatake S, Maruhashi A: **Improvement effect on the depth-dose distribution by CSF drainage and air infusion of a tumour-removed cavity in boron neutron capture therapy for malignant brain tumours.** *Phys Med Biol* 2006, **51**:1173-83.
12. Wu G, Barth RF, Yang W, Lee RJ, Tjarks W, Backer MV, Backer JM: **Boron containing macromolecules and nanovehicles as delivery agents for neutron capture therapy.** *Anticancer Agents Med Chem* 2006, **6**:167-84.
13. Mehta SC, Lu DR: **Targeted drug delivery for boron neutron capture therapy.** *Pharm Res* 1996, **13**:344-51.
14. Maruyama K, Ishida O, Kasaoka S, Takizawa T, Utoguchi N, Shinohara A, Chiba M, Kobayashi H, Eriguchi M, Yanagie H: **Intracellular targeting of sodium mercaptoundecahydrododecaborate (BSH) to solid tumors by transferrin-PEG liposomes, for boron neutron-capture therapy (BNCT).** *J Control Release* 2004, **98**:195-207.
15. Masunaga S, Kasaoka S, Maruyama K, Nigg D, Sakurai Y, Nagata K, Suzuki M, Kinashi Y, Maruhashi A, Ono K: **The potential of transferrin-pendant-type polyethyleneglycol liposomes encapsulating decahydrodecaborate-(^{10})B (GB-10) as (^{10})B-carriers for boron neutron capture therapy.** *Int J Radiat Oncol Biol Phys* 2006, **66**:1515-22.
16. Doi A, Kawabata S, Iida K, Yokoyama K, Kajimoto Y, Kuroiwa T, Shirakawa T, Kirihata M, Kasaoka S, Maruyama K, Kumada H, Sakurai Y, Masunaga S, Ono K, Miyatake S: **Tumor-specific targeting of sodium boro capta te (BSH) to malignant glioma by transferrin-PEG liposomes: a modality for boron neutron capture therapy.** *J Neurooncol* 2008, **87**:287-94.
17. Aljabili MR, Lodato F, Burroughs AK: **Surveillance and diagnosis for hepatocellular carcinoma.** *Liver Transpl* 2007, **13(11 Suppl 2)**:S2-12.
18. World Health Organization: **World Health Statistics 2008/Future trends in global mortality.**[http://www.who.int/whosis/whostat/2008/en/index.html].
19. Arciero CA, Sigurdson ER: **Diagnosis and treatment of metastatic disease to the liver.** *Semin Oncol* 2008, **35**:147-59.
20. Kaneda Y, Nakajima T, Nishikawa T, Yamamoto S, Ikegami H, Suzuki N, Nakamura H, Morishita R, Kotani H: **Hemagglutinating virus of Japan (HVJ) envelope vector as a versatile gene delivery system.** *Mol Ther* 2002, **6**:219-26.
21. Mima H, Yamamoto S, Ito M, Tomoshige R, Tabata Y, Tamai K, Kaneda Y: **Targeted chemotherapy against intraperitoneally disseminated colon carcinoma using a cationized gelatin-conjugated HVJ envelope vector.** *Mol Cancer Ther* 2006, **5**:1021-8.
22. Kawano H, Komaba S, Kanamori T, Kaneda Y: **A new therapy for highly effective tumor eradication using HVJ-E combined with chemotherapy.** *BMC Med* 2007, **5**:1-7.
23. Kurooka M, Kaneda Y: **Inactivated Sendai virus particles eradicate tumors by inducing immune responses through blocking regulatory T cells.** *Cancer Res* 2007, **67**:227-36.
24. Fujihara A, Kurooka M, Miki T, Kaneda Y: **Intratumoral injection of inactivated Sendai virus particles elicits strong antitumor activity by enhancing local CXCL10 expression and systemic NK cell activation.** *Cancer Immunol Immunother* 2008, **57**:73-84.
25. Mima H, Tomoshige R, Kanamori T, Tabata Y, Yamamoto S, Ito S, Tamai K, Kaneda Y: **Biocompatible polymer enhances the in vitro and in vivo transfection efficiency of HVJ envelope vector.** *J Gene Med* 2005, **7**:888-97.
26. Asai T, Ueda T, Itoh K, Yoshioka K, Aoki Y, Mori S, Yoshikawa H: **Establishment and characterization of a murine osteosarcoma cell line (LM8) with high metastatic potential to the lung.** *Int J Cancer* 1998, **76**:418-422.
27. Lee CM, Tanaka T, Murai T, Kondo M, Kimura J, Su W, Kitagawa T, Ito T, Matsuda H, Miyasaka M: **Novel chondroitin sulfate-binding cationic liposomes loaded with cisplatin efficiently suppress the local growth and liver metastasis of tumor cells in vivo.** *Cancer Res* 2002, **62**:4282-8.
28. Fukunaka Y, Iwanaga K, Morimoto K, Kakemi M, Tabata Y: **Controlled release of plasmid DNA from cationized gelatin hydrogels based on hydrogel degradation.** *J Control Release* 2002, **80**:333-43.
29. Hosseinkhani H, Aoyama T, Ogawa O, Tabata Y: **Ultrasound enhancement of in vitro transfection of plasmid DNA by a cationized gelatin.** *J Drug Target* 2002, **10**:193-204.
30. Nagata I, Kimura Y, Ito Y, Tanaka T: **Temperature-Sensitive Phenomenon of Viral Maturation Observed in BHK Cells Persistently Infected with HVJ.** *Virology* 1972, **49**:453-461.
31. Guttenberger M: **Protein Determination.** *Cell Biology* A Laboratory Handbook:295-303.
32. Ogura K, Yanagie H, Eriguchi M, Lehmann EH, Kuhne G, Bayon G, Kobayashi H: **Neutron capture autoradiographic study of the biodistribution of ^{10}B in tumor-bearing mice.** *Appl Radiat Isot* 2004, **61**:585-90.
33. Saga K, Tamai K, Kawachi M, Shirnbo T, Fujita H, Yamazaki T, Kaneda Y: **Functional modification of Sendai virus by siRNA.** *J Biotechnol* 2008, **133**:386-94.
34. Maeda H, Wu J, Sawa T, Matsumura Y, Hori K: **Tumor vascular permeability and the EPR effect in macromolecular therapeutics: a review.** *J Control Release* 2000, **65**:271-84.
35. Siwak DR, Tari AM, Lopez-Berestein G: **The potential of drug-carrying immunoliposomes as anticancer agents. Commentary re: J. W. Park et al., Anti-HER2 immunoliposomes: enhanced efficacy due to targeted delivery.** *Clin Cancer Res* 2002, **8**:1172-1181, Clin Cancer Res 2002;8:955-6.
36. Yanagie H: **Selective Enhancement of Boron Accumulation with Boron-Entrapped Water-in-oil-in-water Emulsion in VX-2 Rabbit Hepatic Cancer Model for BNCT.** Proc of 12th International Congress of Neutron Capture Therapy; 2006.
37. Ye SJ: **Monte Carlo based protocol for cell survival and tumour control probability in BNCT.** *Phys Med Biol* 1999, **44**:447-61.
38. Kobayashi T, Kanda K: **Analytical calculation of boron- 10 dosage in cell nucleus for neutron capture therapy.** *Radiat Res* 1982, **91**:77-94.
39. Kinashi Y, Masunaga S, Nagata K, Suzuki M, S T, Ono K: **A bystander effect observed in boron neutron capture therapy: A study of the induction of mutations in the HPRT locus.** *Int J Radiat Oncol Biol Phys* 2007, **68**:508-14.
40. Suzuki M, Sakurai Y, Masunaga S, Kinashi Y, Nagata K, Ono K: **Dosimetric study of boron neutron capture therapy with borocaptate sodium (BSH)/lipiodol emulsion (BSH/lipiodol-BNCT) for treatment of multiple liver tumors.** *Int J Radiat Oncol Biol Phys* 2004, **58**:892-6.
41. Suzuki M, Nagata K, Masunaga S, Kinashi Y, Sakurai Y, Maruhashi A, Ono K: **Biodistribution of ^{10}B in a rat liver tumor model following intra-arterial administration of sodium borocaptate (BSH)/degradable starch microspheres (DSM) emulsion.** *Appl Radiat Isot* 2004, **61**:933-7.
42. Yanagie H, Tomita T, Kobayashi H, Fujii Y, Nonaka Y, Saegusa Y, Hasumi K, Eriguchi M, Kobayashi T, Ono K: **Inhibition of human pancreatic cancer growth in nude mice by boron neutron capture therapy.** *Br J Cancer* 1997, **75**:660-5.
43. Yanagie H, Sakurai Y, Ogura K, Kobayashi T, Furuya Y, Sugiyama H, Kobayashi H, Ono K, Nakagawa K, Takahashi H, Nakazawa M, Eriguchi M: **Evaluation of neutron dosimetry on pancreatic cancer phantom model for application of intraoperative boron neutron-capture therapy.** *Biomed Pharmacother* 2007, **61**:505-14.
44. Suzuki M, Sakurai Y, Masunaga S, Kinashi Y, Nagata K, Maruhashi A, Ono K: **A preliminary experimental study of boron neutron capture therapy for malignant tumors spreading in thoracic cavity.** *Jpn J Clin Oncol* 2007, **37**:245-9.
45. Kawano H, Komaba S, Yamasaki T, Maeda M, Kimura Y, Maeda A, Kaneda Y: **New potential therapy for orthotopic bladder carcinoma by combining HVJ envelope with doxorubicin.** *Cancer Chemother Pharmacol* 2008, **61**:973-8.

doi:10.1186/1748-717X-6-8
Cite this article as: Fujii *et al.*: Cationized gelatin-HVJ envelope with sodium borocaptate improved the BNCT efficacy for liver tumors *in vivo*. *Radiation Oncology* 2011 **6**:8.

Clinical Effectiveness of Boron Neutron Capture Therapy for a Recurrent Malignant Peripheral Nerve Sheath Tumor in the Mediastinum

Masayoshi Inoue, MD, PhD, Chun Man Lee, MD, PhD,† Koji Ono, MD, PhD,‡ Minoru Suzuki, MD, PhD,‡ Toshiteru Tokunaga, MD,* Yoshiki Sawa, MD, PhD,† and Meinoshin Okumura, MD, PhD**

A 70-year-old woman underwent extirpation of a malignant peripheral nerve sheath tumor, 4.5 × 2.0 cm in size, in the right supraclavicular fossa. Locoregional recurrence was found 10 months after operation (Figure 1). Although one course of systemic chemotherapy using cisplatin (80 mg/m^2 at day 1) and vinorelbine (25 mg/m^2 at days 1 and 8) was given, the recurrent tumor progressed. Because conventional radiotherapy is not effective for malignant peripheral nerve sheath tumor, boron neutron capture therapy (BNCT) was considered based on the subcutaneous mediastinal location. After institutional review board approval and securing the patient's written informed consent, accumulation of p-boronophenylalanine (BPA) in the tumor was confirmed using 18F-BPA positron emission tomography. Using simulation environment for radiation applications software program, fast neutron and γ-ray physical doses, compound biologic effectiveness- and relative biologic effectiveness-weighted doses, were calculated.

The patient underwent two courses of BNCT with an interval of 3 weeks. BPA-fructose was administered intravenously at a dose of 500 mg/kg just before irradiation. For the first course, the epithermal neutron irradiation was performed for 105 minutes. The dose distribution in the tumor ranged from 13.7 to 22.3 Gy-Eq and was 6.0 Gy-Eq to the skin. For the second course, the irradiation time was shortened to 51 minutes, because of the higher epithermal neutron flux. The dose delivered to the tumor ranged from 6.0 to 24.3 Gy-Eq and was 9.7 Gy-Eq to the skin.

Chest computed tomography scan 1 year after BNCT showed that the tumor size decreased from 6.2 × 4.0 cm to 4.6 × 3.2 cm in size (25% reduction), and stable disease was maintained for 24 months (Figure 2). Positron emission tomography-computed tomography 18 months after BNCT showed no uptake of 18F-fluorodeoxy glucose in the residual mass, suggesting no viability (Figure 3). Neuralgia of the right arm improved. Although temporary dysphagia because of an oral mucosa disorder was observed as a side effect, the patient's general quality of life was preserved. There is no evidence of recurrence 2 years after BNCT.

DISCUSSION

When ^{10}Boron absorbs thermal neutrons, α and ^{7}Lithium particles are generated.[1] BNCT selectively injures the tumor cells containing ^{10}Boron; it was suitable in this case with tumor invasion into the neighboring great vessels. Because the peak of thermal neutron flux is 3 cm beneath the tissue surface, its clinical applications have been limited to malignant melanomas and brain tumors. Kato et al.[2] reported its efficacy for head and neck malignancies. The indication was extended to metastatic liver tumor,[3] malignant mesothelioma,[4] and glioblastoma.[5] This is the first case of mediastinal tumor treated with BNCT.

The effect of BNCT is critically dependent on selective accumulation of ^{10}Boron compounds. The tumor/normal tissue ratio of the ^{10}Boron uptake was 2 in this case, while a ratio greater than 2.5 is preferable for selective treatment. BNCT might be a treatment option for subcutaneous mediastinal tumors, which is resistant to conventional irradiation.

REFERENCES

1. Barth RF, Coderre JA, Vicente MG, et al. Boron neutron capture therapy of cancer: current status and future prospects. *Clin Cancer Res* 2005; 11:3987–4002.
2. Kato I, Ono K, Sakurai Y, et al. Effectiveness of BNCT for recurrent head and neck malignancies. *Appl Radiat Isot* 2004;61:1069–1073.
3. Wittig A, Malago M, Collette L, et al. Uptake of two 10B-compounds in liver metastases of colorectal adenocarcinoma for extracorporeal irradiation with boron neutron capture therapy (EORTC Trial 11001). *Int J Cancer* 2008;122:1164–1171.
4. Suzuki M, Sakurai Y, Masunaga S, et al. Feasibility of boron neutron capture therapy (BNCT) for malignant pleural mesothelioma from a viewpoint of dose distribution analysis. *Int J Radiat Oncol Biol Phys* 2006;66:1584–1589.
5. Vos MJ, Turowski B, Zanella FE, et al. Radiologic findings in patients treated with boron neutron capture therapy for glioblastoma multiforme within EORTC trial 11961. *Int J Radiat Oncol Biol Phys* 2005;61:392–399.

*Department of General Thoracic Surgery, Osaka University Graduate School of Medicine, Suita, Osaka; †Medical Center for Translational Research, Osaka University Hospital, Suita, Osaka; and ‡Radiation Oncology Research Laboratory, Research Reactor Institute, Kyoto University, Kyoto, Japan.

Disclosure: The authors declare no conflicts of interest.

Address for correspondence: Meinoshin Okumura, MD, Department of General Thoracic Surgery, Osaka University Graduate School of Medicine, L5-2-2 Yamadaoka, Suita, Osaka 565-0781, Japan. E-mail: meinosin@thoracic.med.osaka-u.ac.jp

ISSN: 1556-0864/10/0512-2037

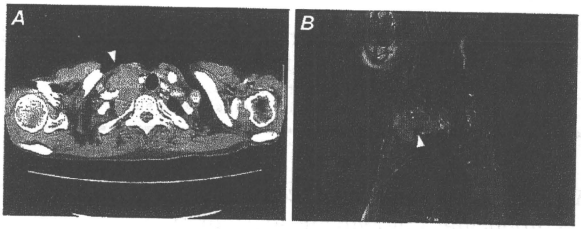

FIGURE 1. Chest computed tomography (CT) scan and magnetic resonance imaging (MRI) showing the recurrent lesion. *A*, Postoperative recurrence, 4.5 × 2.0 cm in size, is seen in the right subclavicular region (arrow head) in the follow-up CT scan 10 months after operation. *B*, Tumor invasion into the right subclavicular artery and brachiocephalic vein is seen (arrow head) in the sagittal view of MRI.

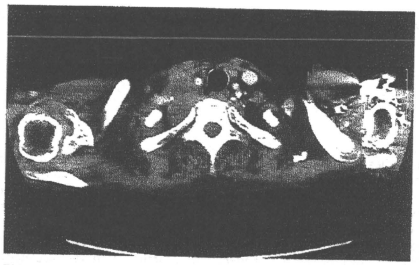

FIGURE 2. Chest computed tomography scan 1 year after boron neutron capture therapy shows shrinkage of the recurrent lesion after chemotherapy from 6.2 × 4.0 cm to 4.6 × 3.2 cm in size (25% reduction).

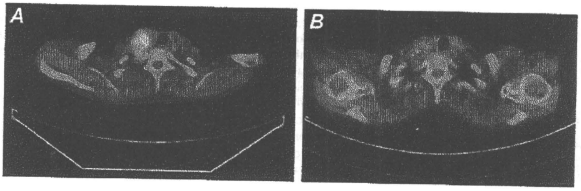

FIGURE 3. FDG-positron emission tomography (PET) shows the remarkable effect of boron neutron capture therapy (BNCT). *A*, PET-computed tomography (CT) before BNCT shows significant tumor uptake. *B*, Although a residual mass is seen, the FDG uptake is reduced to the background level 18 months after BNCT.

Mutation Research 695 (2010) 69–74

Contents lists available at ScienceDirect

Mutation Research/Genetic Toxicology and Environmental Mutagenesis

journal homepage: www.elsevier.com/locate/gentox
Community address: www.elsevier.com/locate/mutres

Ascorbic acid 2-glucocide reduces micronucleus induction in distant splenic T lymphocytes following head irradiation

Yuko Kinashi *, Hiroki Tanaka, Shinichiro Masunaga, Minoru Suzuki, Genro Kashino, Liu Yong, Sentaro Takahashi, Koji Ono

Research Reactor Institute, Kyoto University, Kumatori-cho, Sennan-gun, Osaka 590-0494, Japan

ARTICLE INFO

Article history:
Received 13 April 2009
Received in revised form 2 November 2009
Accepted 6 December 2009
Available online 16 December 2009

Keywords:
Abscopal radiation effect
Ascorbic acid
T lymphocyte
Micronucleus

ABSTRACT

Purpose: Evidence from in vivo studies suggests there are enhanced radiation effects in abscopal regions after local head gamma ray irradiation. Splenocyte apoptosis and T lymphocyte micronuclei were induced at higher rates than what would be estimated given the dose at a shielded, distant position. In addition, we evaluated the radio-protective effects of ascorbic acid, acting as a radical scavenger on enhanced radiation effects in the shielded spleen following local head irradiation.

Methods and materials: The heads of C3H mice were exposed to γ-rays (10–20 Gy), while the other parts of the body were shielded with a 5 cm-thick lead block. The effective dose for the spleen was calculated at 1.0–2.0 Gy. Splenocytes were isolated 24 h after cranial irradiation and their apoptosis was measured with an Elisa kit (Roche). The induction of T lymphocyte micronuclei was studied using the cytokinesis-block micronucleus assay. The ascorbic acid glucoside, 2-O-alpha-D-glucopyranosyl-L-ascorbic acid (AA-2G), was orally administered to mice 1 h before whole body irradiation. The radio protective effects of AA-2G were estimated by comparing the induction of splenocyte damage (by apoptosis) and micronucleus induction.

Results: The splenocyte damage, as measured by the above two methods, was more excessive than what would be expected given exposure to 1.0–2.0 Gy of radiation. Our results suggest that the effects were enhanced in a distant, non-irradiated organ after localized irradiation. Plasma ascorbic acid concentrations were increased 8–10× over control. Treatment with ascorbic acid slightly protected mouse splenocytes from the induction of apoptosis by the enhanced effects of radiation in the abscopal region. However, ascorbic acid significantly inhibited micronucleus induction in splenic T lymphocytes following local head irradiation.

Conclusions: Our results suggest that ascorbic acid effectively scavenged radiation-induced radicals and protected against the enhanced effects of radiation in an abscopal region after local head gamma ray irradiation.

1. Introduction

The abscopal effects of radiation were first reported in 1969 and were defined as significant responses to radiation in tissues that are separate from the area exposed to the radiation [1,2].

The enhanced effects of radiation in shielded organs are thought to be based on the phenomena of so-called bystander effects. Their mechanism is thought to involve radiation signals that are transduced from the radiation-targeted organ to shielded organs [3,4]. Most have been observed in the low-dose range [3,5,6]. In fact, Prise et al. [6] noted that most bystander effects appear to saturate at higher dose levels, and that other factors must switch to hypersensitivity of a non-targeted response.

Abscopal effects from radiation have also been previously reported at therapeutic doses. For example, in studies with partially irradiated lungs, animals and patients were reported to have higher than expected tissue damage in unirradiated parts of the lung [7,8]. The mechanism for this hypersensitivity of non-targeted responses has not been elucidated, but inflammatory responses and reactive oxygen species, such as superoxide radicals, are involved [2,9].

We previously published that bystander effects were observed after boron neutron capture therapy (BNCT), and found that the radical scavenger ascorbate could effectively protect from distant damage [10]. Another group reported that radical scavengers were protective against radiation-induced bystander effects in an in vitro study [11]. Here, we investigated the possibility that 2-O-alpha-D-glucopyranosyl-L-ascorbic acid (AA-2G) had clinically relevant

* Corresponding author. Tel.: +81 72 451 2437; fax: +81 72 451 2627.
E-mail address: kinashi@rri.kyoto-u.ac.jp (Y. Kinashi).

1383-5718/$ – see front matter © 2009 Elsevier B.V. All rights reserved.
doi:10.1016/j.mrgentox.2009.12.002

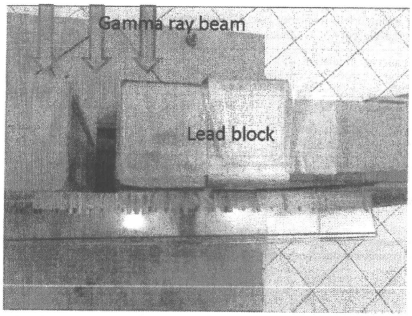

Fig. 1. A view from above showing the strategy for local head irradiation. The head of a mouse was irradiated while being held in a restrainer through a 2 cm slit, while the rest of its body was located behind a 5 cm lead block.

radio-protective effects. Its radio-protective effects were evaluated after induction of apoptosis in mouse splenocytes and micronuclei in splenic T cells, at a site that was distant from local head irradiation.

2. Materials and methods

2.1. Mice and ascorbic acid administration

Six-week-old female C3H/He mice were obtained from Japan Animal Inc. and acclimated to our laboratory for 8–10 weeks prior to use in experiments. AA-2G was purchased from Hayashibara Biochemical Laboratories (Okayama, Japan). C3H female mice (14–16 weeks old) were given AA-2G orally (dissolved in water, 1 mg/g of body weight), 1 h before gamma-ray irradiation. The concentration of AA-2G administration was decided after referencing previous experiments [12–14] and considering the high plasma accumulation and toxicity of ascorbic acid. Note: 1 mg of AA-2G is the equivalent of 0.52 mg of ascorbic acid. The ascorbic acid concentration in mouse plasma after AA-2G administration was measured by HPLC.

2.2. Irradiation

Gamma rays were delivered with a ^{60}Co gamma-ray machine at a rate of 1.0 Gy/min. Mice were restrained in a plastic box on a radiation shelf. For partial head irradiation, heads were placed in a 2.0 cm slit in the front side of the restrainer and the rest of their bodies were shielded behind a 5 cm-thick lead block (Fig. 1). The absorbed doses for the head and the body are shown in Fig. 2. For total body irradiation (to evaluate direct splenic damage following irradiation), the whole body was irradiated (up to 5 Gy).

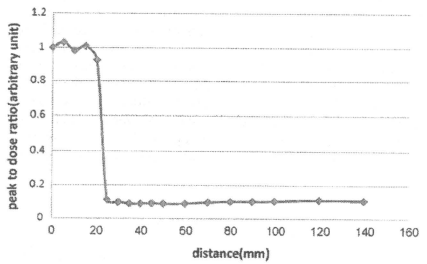

Fig. 2. Estimation of the amount of radiation passing through the 2 cm slit (the irradiated head dose) and into the area shielded by the lead block (the spleen dose). Each point corresponds to a red mark on the scale in Fig. 1. The intervals between the points were 5 mm (0–5 cm), 1 cm (5–10 cm) and 2 cm (10–14 cm). The head of the mouse was located in the first 2 cm (in the open region). The spleen was located at 4 cm. The dose given to the spleen was estimated at 1 Gy when 10 Gy of irradiation was given to the head.

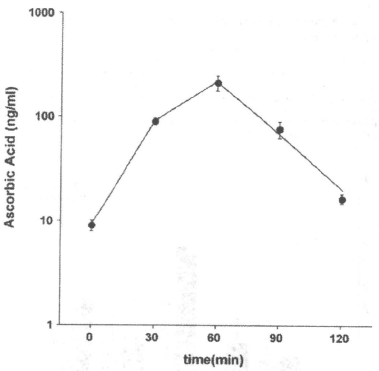

Fig. 3. The concentration of ascorbic acid in mouse plasma after AA-2G administration.

2.3. Isolation of splenocytes and splenic T lymphocytes

Details of the T lymphocyte isolation have been described elsewhere [15]. Briefly, after gamma irradiation, mice were sacrificed by cervical dislocation, and their spleens were removed, minced and washed twice in Hanks' balanced salt solution. Lymphocytes were separated using Ficoll-Hypaque gradients and were resuspended in RPMI 1640 medium (GIBCO) containing 10% fetal calf serum. The T lymphocytes were cultured at 37 °C in a humidified 5% CO_2 incubator. Optimum concentrations of Concanavalin A (Con A, 2 μg/mL) and 2-mercaptoethanol (2-ME, 50 μmol/mL) were used to make lymphocytes transform and divide in culture.

2.4. Radiation induced apoptosis and antioxidant enzyme activation

To determine splenocyte apoptosis, mice were sacrificed 24 h after irradiation and their spleens were removed. Single-cell suspensions were eliminated of erythrocytes by incubating at room temperature for 3 min in a solution of Tris-

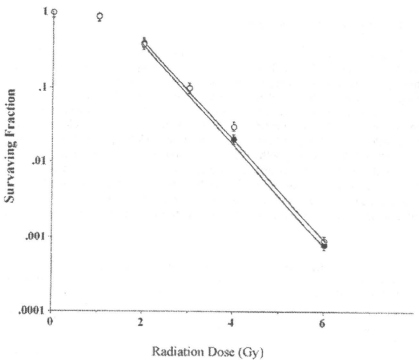

Fig. 4. Survival curves for splenic T lymphocytes following gamma irradiation with (open circle) or without (closed circle) ascorbic acid administration. Data represent the means ± SE of three different independent experiments. The curves for doses greater than 2 Gy were fit by linear regression analysis.

Table 1
Survival parameters for T lymphocytes after gamma ray irradiation with V.C. (ascorbic acid) treatment.

Treatment	D_0	D_{10}
Gamma ray radiation	0.65 ± 0.2 Gy	3.0 ± 0.2 Gy
Gamma ray radiation with V.C. treatment	0.85 ± 0.3 Gy	3.1 ± 0.2 Gy

Data pooled from three or more experiments; mean ± SE. D_0 and D_{10} derived from survival curves following irradiation.

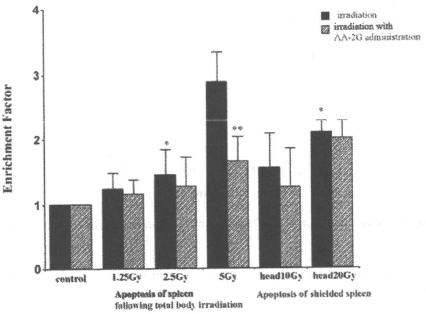

Fig. 5. Induction of apoptosis of mouse splenocytes after irradiation (black bars) and the effect of AA-2G administration (gray bars). Histogram bars show the means ± SE for five animals. (*) Significant increase in apoptosis compared to 2.5 Gy total body irradiation. $p < 0.05$. (**) Significant decrease in apoptosis compared to no ascorbic acid administration. $p < 0.05$.

buffered ammonium chloride. After twice washing with PBS, cells were counted and examined for induction of apoptosis. Apoptosis was detected with a sandwich immunoassay system using a cell death detection ELISA kit (Roche Diagnostic Inc.). The assay is based on the quantitative sandwich enzyme immunoassay principle, using mouse monoclonal antibodies directed against DNA and histones, respectively. Apoptosis was measured by following the ELISA protocol. The enrichment factor was the calculated absorbance of each sample divided by the absorbance of corresponding negative control. To measure the activity of catalase (CAT) and superoxide dismutase (SOD), mouse blood was obtained from the main inferior vein 60, 120 and 1200 min after irradiation. The activities of CAT and SOD in mouse plasma were detected using a colorimetric assay (SRL Research Laboratory Inc., Japan).

2.5. Determination of T lymphocyte survival and the micronucleus assay

Details of the assays for cell survival and micronucleus frequency have been reported previously [15]. Briefly, the survival data for lymphocytes were obtained by limiting dilution assays. To measure the cloning efficiency of lymphocytes, cells were seeded in culture medium (150 μL) at densities of 10–10,000 cells/well in 96-well tissue culture plates. The cloning efficiency was calculated from the proportion of the wells without clones, using limiting dilution analysis [16]. The cytokinesis-block micronucleus assay for lymphocytes was performed following a method described by Fenech and Morley [17] with slight modifications. Cytochalasin B (Sigma) was added to the cultured T lymphocytes at a final concentration of 5.0 μg/mL, 44 h after Con A stimulation. Eighteen hours later, cells were collected by centrifugation and resuspended in Carnoy's fixative. Next, a drop of the cell suspension was spread on a glass slide and dried, the cells were stained with Hoechst 33258 (50 μg/mL), and the frequency of micronuclei was determined on 10 separate slides by counting the total number of micronuclei per 100 binucleated cells.

Table 3
The micronucleus frequency per 100 binucleated T lymphocytes after irradiation and the effect of AA-2G administration.

Total body irradiation (Gy)			Head irradiation 10 Gy
0 Gy	1.25 Gy	2.5 Gy	
2.8 ± 1.5	26.8 ± 6.5	47.9 ± 13.2	62.1 ± 18.5
With AA-2G treatment			
2.9 ± 1.5	14.9 ± 8.5**	29.1 ± 11.5**	24.9 ± 10.5**

Results show the mean ± SE from at least three independent experiments.
** Significant differences were observed with AA-2G administration (Student's *t*-test; $p < 0.05$).

2.6. Statistical analysis

Significance was calculated using Student's tests. Results were considered significant for values of $p < 0.05$.

3. Results

3.1. The effect of ascorbic acid treatment

The ascorbic acid concentration in mouse plasma increased and was maintained at a high level during the 30–90 min after oral administration of AA-2G. One hour after AA-2G administration (1 mg/g of mouse body weight), the concentration of ascorbic acid in the plasma was increased 4–10× over the control (Fig. 3). The plasma level of ascorbic acid increased sharply, as quickly as 30 min, and was maintained at a high level for 1.5 h after oral administration of AA-2G. The availability of AA-2G as ascorbic acid was compatible with a previous report [13].

Fig. 4 and Table 1 show survival curves and the parameters for T lymphocytes after gamma irradiation, with and without ascorbic acid treatment. These results showed that gamma radiation lethality was not affected by ascorbic acid treatment.

3.2. Induction of apoptosis and the activities of anti-oxidative enzymes

Apoptosis was analyzed after 1.25, 2.5 and 5 Gy of whole body irradiation and 10 and 20 Gy of local head irradiation, with and without ascorbic administration. For local head irradiation, the spleen was shielded behind a 5 cm-thick lead block (Fig. 1) and the doses of radiation absorbed by the spleen and head were measured (1.0 Gy for the spleen from 10 Gy of radiation exposure to the head; 2.0 Gy (spleen) from 20 Gy (head); Fig. 2). After 20 Gy head irradiation, the apoptosis that occurred in shielded spleen cells exceeded that which occurred when spleen cells were directly irradiated with 2.5 Gy (Fig. 5). Therefore, the damage to shielded spleen cells was more excessive than what would be expected given a dose of 2.0 Gy.

Fig. 5 also shows the induction of apoptosis in mouse splenocytes after AA-2G treatment. Ascorbic acid protected mouse

Table 2
SOD and catalase activity in mouse serum after treatment with AA-2G.

Time after irradiation (min)	SOD activity (Units/mL)		Catalase activity (Units/mL)	
	6 Gy irradiation	6 Gy irradiation with AA-2G	6 Gy irradiation	6 Gy irradiation with AA-2G
0	7.7 ± 0.8	7.1 ± 0.7	1.0 ± 0.1	1.0 ± 0.1
60	9.2 ± 0.9	10.4 ± 1.0	3.6 ± 0.4	4.2 ± 0.4
120	10.0 ± 0.9	11.0 ± 1.0	3.6 ± 0.4	4.4 ± 0.4
1200	12.5 ± 1.0	14.0 ± 1.4	2.2 ± 0.2	4.4 ± 0.4**

Results show the mean ± SE from at least three independent experiments.
** Significant increases were observed with AA-2G administration (Student's *t*-test; $p < 0.05$).

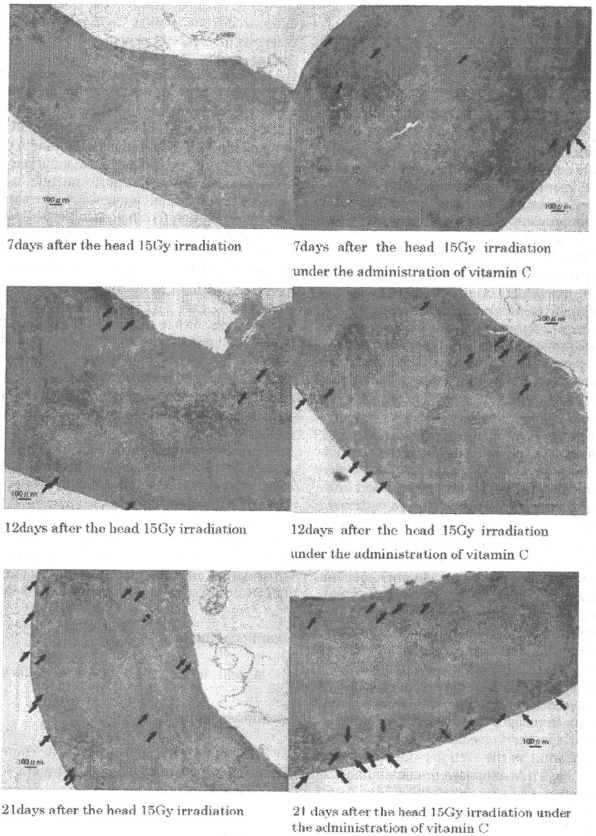

Fig. 6. Spleens 7–21 days after 15 Gy of head irradiation. Formalin-fixed paraffin-embedded tissue sections were HE stained. The arrows show macrophage proliferation in the spleen after the head irradiation (magnification 30×. Scale bars 100 μm).

splenocytes from apoptosis after 5 Gy whole-body irradiation. To understand how anti-oxidative enzymes participate in initial DNA damage, we investigated how treating with AA-2G affected the activation of the CAT and SOD in the plasma following a dose of 6 Gy (1 Gy in addition to the 5 Gy irradiation). AA-2G administration increased the activation of CAT and SOD slightly. A significant increase in CAT activity was observed with AA-2G treatment 20 h after irradiation (Table 2).

3.3. Micronucleus induction

The induction of micronuclei in mouse T lymphocytes after various treatments is shown in Table 3. Micronuclei were counted after 1.25 and 2.5 Gy of whole body irradiation and 10 Gy of local head irradiation, with and without ascorbic administration. As mentioned above, a 10 Gy dose of radiation exposure to the head corresponded to a dose of 1.0 Gy for the shielded spleen. The frequency of micronuclei induced in shielded splenic T cells with 10 Gy of head irradiation was about 2 times higher than that induced after 2.5 Gy of whole body irradiation (Table 3). Our results confirm that shielded, distant splenic T lymphocytes had more damage than what would have been anticipated, given a dose of 1.0 Gy. This again suggests that the radiation effects in a distant, shielded organ were enhanced after local irradiation. However, while treatment with ascorbic acid protected, although not significantly, against the induction of apoptosis in shielded splenocytes, ascorbic acid significantly inhibited shielded splenic T lymphocytes from forming micronuclei after local head irradiation (Fig. 5 and Table 3). Therefore, unlike its effects on induction of mouse splenocyte apoptosis, AA-2G had radioprotective

effects on the induction of T lymphocyte micronuclei after irradiation.

4. Discussion

In high LET therapy, as occurs in boron neutron capture therapy (BNCT) and heavy-ion radiotherapy, hypo-fractionation is acceptable and therapeutic radiation doses are larger than conventional radiotherapies. The normal tissue radiation dose for vascular endothelial cells in BNCT is estimated to be around 10–15 Gy [18]. Enhanced radiation effects in abscopal regions following large local doses of radiation have not previously been investigated. Here, we studied whether shielded splenocytes in abscopal regions suffered enhanced radiation effects after 10–20 Gy of local head gamma ray-irradiation. Splenocyte apoptosis induction and T lymphocyte micronuclei were higher than what would be expected with the estimated dose of radiation in the distant, shielded spleen.

In vivo radiation-induced bystander effects are defined as phenomena that occur when irradiation signals are transduced from an irradiated lesion to a shielded organ and induce a radiation effect in that non-irradiated, shielded organ. A previous group reported that the spleen is a target organ of local-irradiation induced bystander effects in vivo. Koturbash et al. described how cranial X-ray irradiation (1 Gy) induced DNA damage, apoptosis, and increased p53 levels in a shielded spleen [5]. They also suggested the possibility that the induction of indirect DNA damage in the shielded splenocytes was mediated by reactive oxygen species. Mechanistically, the radiation-induced bystander effect in vivo is thought to be mediated by the inflammatory response after exposure to ionizing radiation. Lorimore et al. reported that macrophage activation following a 4 Gy irradiation provided a mechanism for producing damage via bystander effects [19]. Another previous report showed that tumor cell killing by macrophages was activated with more than 10 Gy [20]. These experiments show that high dose radiation might induce bystander signaling by mediating macrophage activation. We confirmed that large dose local head irradiation (10–20 Gy) induced apoptosis and micronuclei in the distant, shielded spleen. These enhanced radiation effects in an abscopal region were induced by a large dose irradiation and may have been mediated by macrophage activation. Shown in the left column of Fig. 6, histological sections revealed macrophage proliferation in the spleen appearing on the 12th day post-irradiation and becoming severe by day 21. Macrophage proliferation in the spleen was found to be more severe after ascorbic acid administration, and to occur earlier (on the 7th day post-irradiation; shown in the right column of Fig. 6).

We evaluated the protective effects of a radical scavenger on enhanced radiation effects in the distant spleen after large doses of local head irradiation. Free radicals are one of the most important bio-chemicals that are triggered by the activation of macrophages following irradiation [21]. This suggests the possibility that radical scavengers might protect abscopal regions from enhanced radiation effects. Our study of apoptosis induction suggests that AA-2G treatment suppressed the induction of apoptosis following total body radiation. In our anti-oxidative enzyme study, AA-2G administration increased catalase activity after 20 h, which was the length of the apoptosis assay, but AA-2G did not significantly affect SOD activity. The C3H/He mouse strain is more radiation-resistant than other Balb/c mouse strains [22,23]. The different sensitivities of mouse strains to irradiation were determined by micronucleus formation in T lymphocytes and fibroblasts, and an intestinal cell survival assay [15]. A previous report demonstrated that hepatic CAT and SOD enzyme activities increased 30 min after whole body ionizing irradiation of C3H mice, suggesting that CAT and SOD may be related to the mechanism of their radiation resistance [24]. We confirmed that these antioxidant enzymes had elevated activities after irradiation and that AA-2G enhanced CAT activity. This result suggests that ascorbic acid may protect from radiation damage by inducing CAT.

We previously reported that radical scavengers are protective against neutron-induced mutations [25,26]. Furthermore, we compared the effects of DMSO (a source of short-lived radical scavengers) and ascorbic acid (a source of long-lived radical scavengers) on the induction of mutations in bystander cells. DMSO treatment slightly reduced the frequency of mutations that were induced by the bystander effect, but post-radiation ascorbic-acid treatment reduced the mutation frequency more than DMSO [10]. Recently, Harada et al. reported that ascorbic acid was an effective radical scavenger for suppressing the bystander response in vitro. They examined three types of radical scavengers, including a nitric oxide scavenger, and found that ascorbic acid was the most effective suppressor of micronucleus induction in non-irradiated bystander cells [27].

We showed that ascorbic acid significantly inhibited shielded splenic T lymphocytes from forming micronuclei following local head irradiation (Fig. 5 and Table 3). However, AA-2G did not protect shielded splenocytes against apoptosis. These results show that AA-2G treatment had radio-protective effects on T-lymphocytes in abscopal regions (in the spleen), but this did not apply to all splenic cells.

Clinically, chromosomal instability [28] and epigenetic dysregulation of DNA [29] were analyzed in non-irradiated or distant organs after irradiation. Enhanced radiation effects in abscopal regions are thought to increase the incidence of secondary, post-radiation therapy cancers. Therefore, effective radioprotection from enhanced radiation effects in abscopal regions is needed. Ascorbic acid is a well-known, important vitamin and a non-toxic radical scavenger that can be effective for protecting against enhanced radiation effects in abscopal regions during radiation therapy.

Conflict of interest

Authors declare that there are no conflicts of interest.

Acknowledgments

This study was supported by a Grant-in-Aid for Scientific Research from the Ministry of Education, Culture, Sports, Science and Technology of Japan.

References

[1] M.P. Nobler, The abscopal effect in malignant lymphoma and its relationship to lymphocyte circulation, Radiology 93 (1969) 410–412.
[2] W.F. Morgan, Non-targeted and delayed effects of exposure to ionizing radiation: II. Radiation-induced genomic instability and bystander effects in vivo, clastogenic factors and transgenerational effects, Radiat. Res. 159 (2003) 581–596.
[3] K. Camphausen, M.A. Moses, C. Menard, M. Sproull, W.D. Beecken, J. Folkman, M.S. O'Reilly, Radiation abscopal antitumor effect is mediated through p53, Cancer Res. 63 (2003) 1990–1993.
[4] E.I. Azzam, J.B. Little, The radiation-induced bystander effect: evidence and significance, Hum. Exp. Toxicol. 23 (2004) 61–65.
[5] I. Koturbash, J. Loree, K. Kutanzi, C. Koganow, I. Pogribny, O. Kovalchuk, In vivo bystander effect: cranial X-irradiation leads to elevated DNA damage, altered cellular proliferation and apoptosis, and increased p53 levels in shielded spleen, Int. J. Radiat. Oncol. Biol. Phys. 70 (2007) 554–562.
[6] K.M. Prise, M. Folkard, B.D. Michael, A review of the bystander effect and its implications for low-dose exposure, Radiat. Protect. Dosimetry 104 (2003) 347–355.
[7] G.W. Morgan, S.N. Breit, Radiation and the lung: a re-evaluation of the mechanism mediating pulmpnary injury, Int. J. Radiat. Oncol. Biol. Phys. 31 (1995) 361–369.
[8] M.A. Khan, R.P. Hill, J. Van Dyk, Partial volume rat lung irradiation: an evaluation of early DNA damage, Int. J. Radiat. Oncol. Biol. Phys. 40 (1998) 467–476.

[9] K.M. Prise, M. Folkard, B.D. Michael, Bystander response induced by low LET radiation, Oncogene 22 (2003) 7043–7049.
[10] Y. Kinashi, S. Masunaga, K. Nagata, M. Suzuki, S. Takahashi, K. Ono, A bystander effect observed in boron neutron capture therapy: a study of the induction of mutations in the HPRT locus, Int. J. Radiat. Oncol. Biol. Phys. 68 (2007) 508–514.
[11] G. Kashino, K.M. Prise, K. Suzuki, N. Matsuda, S. Kodama, M. Suzuki, K. Nagata, Y. Kinashi, S. Masunaga, K. Ono, M. Watanabe, Effective suppression of bystander effects by DMSO treatment of irradiated CHO cells, J. Radiat. Res. 48 (2007) 197–204.
[12] I. Yamamoto, S. Suga, Y. Mitoh, M. Tanaka, N. Muto, Antiscorbutic activity of L-ascorbic acid 2-gluciside and its availability as a vitamin C supplement in normal rats and guinea pigs, J. Pharmacobiodyn. 13 (1990) 688–695.
[13] A. Tai, Y. Fujitani, K. Matsumoto, D. Kawasaki, I. Yamamoto, Bioability of a series of novel acylated ascorbic acid derivatives, 6-O-acyl-2-O-α-D-glucopyranosyl-L-ascorbic acids, as an ascorbic acid supplement in rats and guinea pigs, Biosci. Biotechnol. Biochem. 66 (2002) 1628–1634.
[14] L.V. d'Uscio, S. Milstien, D. Richardson, L. Smith, Z.S. Katusic, Long-term Vitamin C treatment increase vascular tetrahydrobiopterin levels and nitric oxide synthase activity, Circulat. Res. 92 (2003) 88–95.
[15] Y. Kinashi, K. Ono, M. Abe, The micronucleus assay of lymphocytes is a useful predictive assay of the radiosensitivity of normal tissue: a study of three inbred strains of mice, Radiat. Res. 148 (1997) 341–347.
[16] H. Waldmann, S. Cobbold, I. Lefkovits, Limiting dilution analysis, in: G.G.B. Klaus (Ed.), Lymphocytes, A Practical Approach, IRL, Oxford, 1987, pp. 163–188.
[17] F. Fenech, A.A. Morley, Cytokinesis-block micronucleus method in human lymphocytes: effect of in vivo aging and low dose X-irradiation, Mutat. Res. 161 (1986) 193–198.
[18] T. Kageji, S. Nagahiro, S. Uyama, Y. Mizobuchi, Y. Nakagawa, Clinical review of BNCT using mixed neutron beam in patients with malignant glioma, in: W. Sauerwein, R. Moss, A. Wittig (Eds.), Research and Development in Neutron Capture Therapy Monduzzi Editore S.p.A., Bologna, Italy, 2002, pp. 1085–1091.
[19] S.A. Lorimore, P.J. Coates, G.E. Scobie, G. Milne, E.G. Wright, Inflammatory-type responses after exposure to ionizing radiation in vivo: a mechanism for radiation-induced bystander effects? Oncogene 20 (2001) 7085–7095.
[20] L.E. Lambert, D.M. Paulnock, Modulation of macrophage function by γ-irradiation; Acquisition of the primed cell intermediate stage of macrophage tumoricidal action pathway, J. Immunol. 139 (1987) 2834–2841.
[21] G. McLennan, L.W. Oberley, A.P. Author, The role of oxygen-derived free radicals in radiation-induced damage and death of nondividing eukaryotic cells, Radiat. Res. 84 (1980) 122–132.
[22] K.H. Kohn, M.M. Kallman, The influence of strain on acute X-ray lethality in the mouse: LD50 and death rate studies, Radiat. Res. 5 (1956) 309–317.
[23] T.H. Roderic, The response of twenty-seven inbred strains of mice to daily doses of whole-body X-irradiation, Radiat. Res. 120 (1963) 631–639.
[24] R. Hardmeier, H. Hoeger, S. Fang-Kircher, A. Khoschsorur, G. Lubic, Transcription and activity of antioxidant enzymes after ionizing irradiation in radiation-resistant and radiation-sensitive mice, Proc. Natl. Acad. Sci. U.S.A. 94 (1997) 7572–7576.
[25] Y. Kinashi, Y. Sakurai, S. Masunaga, M. Suzuki, M. Akaboshi, K. Ono, Dimethyl sulfoxide protects against thermal and epithermal neutron-induced cell death and mutagenesis of Chinese hamster ovary (CHO) cells, Int. J. Radiat. Oncol. Biol. Phys. 47 (2000) 1371–1378.
[26] Y. Kinashi, Y. Sakurai, S. Masunaga, M. Suzuki, K. Nagata, K. Ono, Ascorbic acid reduced mutagenicity at the HPRT locus in CHO cells against thermal neutron radiation, Appl. Radiat. Isotopes 61 (2004) 929–932.
[27] T. Harada, G. Kashino, K. Suzuki, N. Matsuda, S. Kodama, M. Watanabe, Different involvement of radical species in irradiated and bystander cells, Int. J. Radiat. Biol. 84 (2008) 809–814.
[28] E. Gwyneth, S.A. Watson, A. Lorimore, D.A. Macdonald, E.G. Wright, Chromosomal instability in unirradiated cells induced in vivo by a bystander effect of ionizing radiation, Cancer Res. 60 (2000) 5608–5611.
[29] I. Koturbash, A. Boyko, R. Rodriguez-Juarez, R.J. MacDonald, V.P. Tryndyak, I. Kovalchuk, I.P. Pogribny, O. Kovalchuk, Role of epigenetic effects in maintenance of long-term persistent bystander effect in spleen in vivo, Carcinogenesis 28 (2007) 1831–1838.